6-2016

Meox2 haploinsufficiency increases neuronal cell loss in a mouse model of Alzheimer's disease

Ileana Soto Reyes
Rowan University, sotoreyes@rowan.edu

Weronika A. Grabowska

Kristen D. Onos

Leah C. Graham

Harriet M. Jackson

See next page for additional authors

Neurobiology of Aging 42 (2016) 50–60

Contents lists available at ScienceDirect

Neurobiology of Aging

journal homepage: www.elsevier.com/locate/neuaging

Meox2 haploinsufficiency increases neuronal cell loss in a mouse model of Alzheimer's disease

Ileana Soto [a,b,c], Weronika A. Grabowska [a,d], Kristen D. Onos [a], Leah C. Graham [a,e], Harriet M. Jackson [a], Stephen N. Simeone [a], Gareth R. Howell [a,e,*]

[a] The Jackson Laboratory, Bar Harbor, ME, USA
[b] Department of Biological Science, Rowan University, Glassboro, NJ, USA
[c] Department of Biomedical and Translational Sciences, Rowan University, Glassboro, NJ, USA
[d] College of the Atlantic, Bar Harbor, ME, USA
[e] Graduate Program in Genetics, Sackler School of Graduate Biomedical Sciences, Tufts University, Boston, MA, USA

ARTICLE INFO

Article history:
Received 24 October 2015
Received in revised form 10 February 2016
Accepted 20 February 2016
Available online 2 March 2016

Keywords:
Neurovascular remodeling
Neurodegeneration
Aging
Neurovascular deficits

ABSTRACT

Evidence suggests that multiple genetic and environmental factors conspire together to increase susceptibility to Alzheimer's disease (AD). The amyloid cascade hypothesis states that deposition of the amyloid-β (Aβ) peptide is central to AD; however, evidence in humans and animals suggests that Aβ buildup alone is not sufficient to cause neuronal cell loss and cognitive decline. Mouse models that express high levels of mutant forms of amyloid precursor protein and/or cleaving enzymes deposit amyloid but do not show neuron loss. Therefore, a double-hit hypothesis for AD has been proposed whereby vascular dysfunction precedes and promotes Aβ toxicity. In support of this, copy number variations in mesenchyme homeobox 2 (*MEOX2*), a gene involved in vascular development, are associated with severe forms of AD. However, the role of *MEOX2* in AD has not been studied. Here, we tested *Meox2* haploinsufficiency in B6.*APP/PS1* (B6.APB^{Tg}) mice, a mouse model of AD. Despite no overt differences in plaque deposition or glial activation, B6.APB^{Tg} mice that carry only one copy of *Meox2* (B6.APB^{Tg}.$Mx^{-/+}$) show increased neuronal cell loss, particularly in regions containing plaques, compared with B6.APB^{Tg} mice. Neuronal cell loss corresponds with a significant decrease in plaque-associated microvessels, further supporting a synergistic effect of vascular compromise and amyloid deposition on neuronal cell dysfunction in AD.

1. Introduction

Alzheimer's disease (AD), a leading cause of dementia, is a complex disease characterized by severe cognitive deficits, neuronal loss, and ultimately death. Accumulation of amyloid-β (Aβ) peptide and plaque deposition in the brain and blood vessel walls are distinctive features of AD that are likely to occur in part as a consequence of neurovascular breakdown (Zlokovic, 2011). Recent evidence supports a significant role of cerebrovascular dysfunction in AD pathogenesis, including severe brain microvascular pathology, angiogenesis impairment, deficits in Aβ peptide clearance through the blood brain barrier (BBB), and cerebral amyloid angiopathy (Brown and Thore, 2011; Farkas and Luiten, 2001; Grammas, 2011; Zlokovic, 2011). In addition, it is known that vascular risk factors such as diabetes, hypertension, obesity, and cardiovascular disease predispose individuals to AD (Dewey and Saz, 2001; Knopman and Roberts, 2010; Norton et al., 2014), possibly by decreasing cerebral blood flow (CBF) and promoting hypoperfusion-hypoxia in the brain (Brown and Thore, 2011; Farkas and Luiten, 2001; Grammas, 2011; Zlokovic, 2011). More importantly, in vivo imaging studies in humans have demonstrated that early cerebrovascular hypoperfusion precedes Aβ accumulation and brain atrophy in AD and is associated with cognitive decline (Iadecola, 2004; Knopman and Roberts, 2010; Zlokovic, 2011), suggesting that early neurovascular pathology and dysfunction lead to neuronal failure and neurodegeneration.

In recent years, increasing evidence in animal models and human brains from AD patients have demonstrated how molecular and cellular events that lead to neurovascular dysfunction influence and interact with other pathologic processes in AD, including Aβ accumulation and tau pathology (Halliday et al., 2015; Sagare et al., 2013; Sengillo et al., 2013; Winkler et al., 2015; Zhao et al., 2015). It has been found that genetically induced loss of pericytes in amyloid precursor protein (APP)-overexpressing mice causes BBB breakdown, increased levels of Aβ plaque deposition, and extensive loss of neurons (Sagare et al., 2013). In addition, extensive loss of

* Corresponding author at: The Jackson Laboratory, 600 Main St, Bar Harbor, Maine, 04609, USA. Tel.: +1 (207) 288 6572; fax: +1 (207) 288 6078.
E-mail address: gareth.howell@jax.org (G.R. Howell).

http://dx.doi.org/10.1016/j.neurobiolaging.2016.02.025

pericytes and BBB breakdown were evident in human brains from AD patients carrying the apolipoprotein E4 (APOE4) gene (Halliday et al., 2015). Also, reduced expression of *PICALM*, a genetic risk factor for AD, is associated with reductions in clearance of Aβ and cognitive impairments (Zhao et al., 2015). More recently, it was found that genetic reduction of the glucose transporter GLUT1 in brain endothelial cells from mice overexpressing APP caused BBB breakdown, increased levels of Aβ plaque deposition, and significant neuronal loss (Winkler et al., 2015). Collectively, these studies strongly support an early and significant role of neurovascular disruption in AD onset and progression. In line with these findings, a two-hit vascular hypothesis has been proposed, postulating that vascular risk factors (that are increased by age) induce BBB breakdown and/or hypoperfusion, thus disrupting Aβ clearance and neurotoxicity (Zlokovic, 2011). Aβ deposition may also amplify the neurovascular injury by disrupting angiogenic responses in brain endothelial cells and promoting blood vessel elimination, leading to neuronal dysfunction and neurodegeneration (Brown and Thore, 2011; Grammas et al., 2011).

Genetic risk factors are important contributors to AD development. A recent genome-wide association study identified rare copy number variations associated with early and severe phenotypes of AD (Rovelet-Lecrux et al., 2012). The study identified copy number variations in the homeobox protein mesenchyme homeobox 2 (*MEOX2*), a gene expressed by the vascular system that plays a major role in vascular differentiation (Gorski and Walsh, 2003). *MEOX2* expression is downregulated in brain endothelial cells from AD patients, and reduced levels of MEOX2 cause aberrant angiogenic responses in human and mouse endothelial cells (Wu et al., 2005). However, the impact of *Meox2* haploinsufficiency in mouse models of AD remains to be tested.

As copy number variations in *MEOX2* are associated with early and severe phenotypes of AD, in this study, the contribution of *Meox2* haploinsufficiency (i.e., one copy of *Meox2*) to AD pathology in C57BL/6J.$APP^{swe}PSEN1^{de9}$ (Jankowsky et al., 2004, herein referred to as B6.APB^{Tg}) mice was assessed. B6.APB^{Tg} mice haploinsufficient for *Meox2* presented significant neuronal degeneration and cognitive decline that correlated with a loss of microvessels, particularly in regions of Aβ plaque deposition. This suggests that *Meox2* haploinsufficiency may sensitize endothelial cells to Aβ toxicity and further supports a contribution of vascular dysfunction to AD susceptibility and pathology.

2. Materials and methods

2.1. Mouse strains and cohort generation

All experiments involving mice were conducted in accordance with policies and procedures described in the Guide for the Care and Use of Laboratory Animals of the National Institutes of Health and were approved by the Institutional Animal Care and Use Committee at The Jackson Laboratory. All mice were bred and housed in a 12/12 hour light/dark cycle. All experiments were performed on a unified genetic background (C57BL/6J). C57BL/6J mice heterozygous for the insertion of the cre-recombinase gene in place of the *Meox2* gene were obtained from The Jackson Laboratory (B6.129S4-$Meox2^{CreSor}$, JAX stock #003755). The Cre insertion ablates the transcription of the *Meox2* gene creating a *Meox2* null allele ($Mx^{-/+}$). C57BL/6J.$APP^{swe}Psen1^{de9}$ mice (B6.Cg-Tg(APPswe, PSEN1dE9)85Dbo/Mmjax, JAX stock #005864), referred to in this study as B6.APB^{Tg} mice, were obtained from the Mutant Mouse Resource and Research Center at The Jackson Laboratory.

To produce experimental animals, $Mx^{-/+}$ mice were crossed with B6.APB^{Tg} mice and aged. For the Y-maze task, cohorts of 8–10 mice for each of the 4 genotypes were established and aged to 14 months. For postmortem characterization of AD phenotypes, brains from 2 males and 2 females at 10 and 14 months (a total of 8 mice per genotype, 32 mice in total) were assessed. Mouse brains were also examined at 4 months of age to determine early changes in microvascular density because of *Meox2* haploinsufficiency. Although disease onset and early progression are greater in female B6.APB^{Tg} mice, in our colony, no differences in AD phenotypes are observed at these later ages (10 and 14 months). Therefore, data from male and female mice were combined.

2.2. Spatial working memory tests using the Y-maze

Behavioral tests were performed in the Mouse Neurophenotyping Behavioral Facility at The Jackson Laboratory. To test spatial working memory, spontaneous alternation behavior was assessed using the Y-maze test. Each group of mice was compared with the other experimental/control groups and also to chance levels (50%) as reported by others (Bertholet and Crusio, 1991; Hooper et al., 1996; Jacquelin et al., 2012). At the beginning of trials, mice were placed midway in the start arm and allowed to freely explore the 3 arms for 8 minutes. The sequence of arm entries was recorded by a ceiling-mounted video camera and analyzed with Ethovision software (Noldus). The maze was cleaned with 1% Virkon before the tests began and between animals to eliminate traces of odor. The number of arm entries and the number of triads (defined as entries into the 3 different arms of the Y-maze without returning to a previously visited arm, Drew et al., 1973; Hughes, 2004) were recorded to calculate the alternation percentage. Only mice that performed >20 arm entries were included in the analysis, to ensure that animals were engaged in active exploration of the maze.

2.3. Tissue harvesting, protein isolation, and sectioning

Mice were administered a lethal dose of ketamine/xylazine by intraperitoneal injection, in accordance to Institutional Animal Care and Use Committee protocols, and transcardially perfused with 1× phosphate-buffered saline (PBS) at 4, 10, and 14 months of age. Brains were then dissected, the right hemisphere was snap frozen for protein isolation, and the left hemisphere was fixed in 4% paraformaldehyde overnight at 4 °C, rinsed with 1× PBS, cryoprotected first in 10% and then in 30% sucrose at 4 °C, and embedded in optimal cutting temperature compound. Frozen brains were sectioned at 20 μm and stored at −80 °C until required. Protein (for 6E10 and human $A\beta_{42}$ measurements) was extracted with Trizol Reagent (Life Technologies cat#15596–018) following manufacturer's guidelines. Pellets were resuspended in a solution of 1:1 8M urea and 1% sodium dodecyl sulfate. Additional samples were extracted via RIPA lysis buffer (Sigma-Aldrich) for MEOX2 Western blots.

2.4. Immunofluorescence and Thioflavin S staining

Brain sections were incubated 2 nights at 4 °C in the following primary antibodies: goat polyclonal anti-CD31 (1:40; R&D Systems), Biotinylated Lycoperiscon Esculentum (Tomato) Lectin (1:200; Vector), chicken polyclonal anti-glial fibrillary acidic protein (GFAP) (1:200; Acris Antibodies), rabbit polyclonal anti-IBA1 (also known as allograft inflammatory factor [AIF1]) (1:200; Wako), rat monoclonal CD68 (1:200; AbD Serotec), sheep polyclonal TREM2 (1:100; R&D Systems), laminin A2 (LAMA2) (1:100; Abcam), and mouse anti NEUN (1:200; Millipore). All antibodies were diluted in 1× PBS and 1% TritonX-100 containing 10% normal donkey serum. After primary incubation, sections were washed 3 times in 1× PBS and 1% TritonX-100 and incubated with their respective secondary antibody (donkey anti-chicken Alexa Fluor 633, donkey anti-rabbit Alexa Fluor 488/594, donkey anti-goat Alexa Fluor 488/594, donkey

anti-rat Alexa Fluor 594, donkey anti-mouse Alexa Fluor 488/633, Streptavidin Alexa 488/633, 1:1000 dilution; Life Technologies) for 2 hours at room temperature. All sections were then counterstained with 4',6-diamidino-2-phenylindole and mounted with Aqua Poly-Mount. For Thioflavin S staining, sections stained with antibodies raised against IBA1 and GFAP or lectin were further counterstained with 1% Thioflavin S (diluted in a 1:1 water:ethanol ratio). Slides were incubated for 8 minutes at room temperature in 1% Thioflavin S, washed in 80% ethanol, then in 95% ethanol, and finally in dH_2O, and mounted. Images were taken using either the Leica SP5 confocal microscope or the Zeiss Axio Imager Z2, located within the Imaging facility at The Jackson Laboratory.

2.5. Image quantitative analyses

Quantifications were performed as follows. For plaque counts, the number of plaques present in the entire cortical region from a central section for each mouse was determined. For quantification of IBA1$^+$ cells in the cortex, 4 images ($\times$20, 1388 $\times$ 1040 microns) were taken for each brain from each mouse with a Zeiss Axio Imager fluorescent microscope, and cells were manually counted using the cell counter plugin from ImageJ (1.47 d) software. For counting NEUN$^+$ cells in the cortex, 4 images ($\times$20, 1388 $\times$ 1040 microns) were randomly taken in similar areas for each brain from each mouse and cropped to 209.63 $\times$ 114.17 microns (including only cortical layers II and III). For quantification of pyramidal neurons in the hippocampus, images of the CA1 region were taken at $\times$63. NEUN$^+$ cells in the cortex and hippocampus images were manually counted with the cell counter plugin from ImageJ (1.47 d) software. All image analyses were performed blind to the experimental conditions. For IBA1$^+$ cells, 3 equally spaced images were captured (using $\times$20 optical lens) of the cortex from a central section of each mouse. For IBA1$^+$ cells surrounding plaques, 6 plaque regions per brain were imaged (using $\times$20 optical lens). Images were processed and cells counted using the cell counter plugin for ImageJ/FIJI. Cells from the 3 images from each mouse were totaled and then averaged across mice. For the analysis of structures surrounding plaques (i.e., CD31$^+$ microvessels, NEUN$^+$ neurons, lectin$^+$, or IBA1$^+$ clusters), images were taken specifically in regions of the cortex that contained plaques in B6.APB^{Tg} and B6.APB^{Tg}.*Mx*$^{-/+}$ brains. Each image was cropped (171.5 $\times$ 159.9 microns) to center on a plaque (to minimize the area within the image not containing plaque).

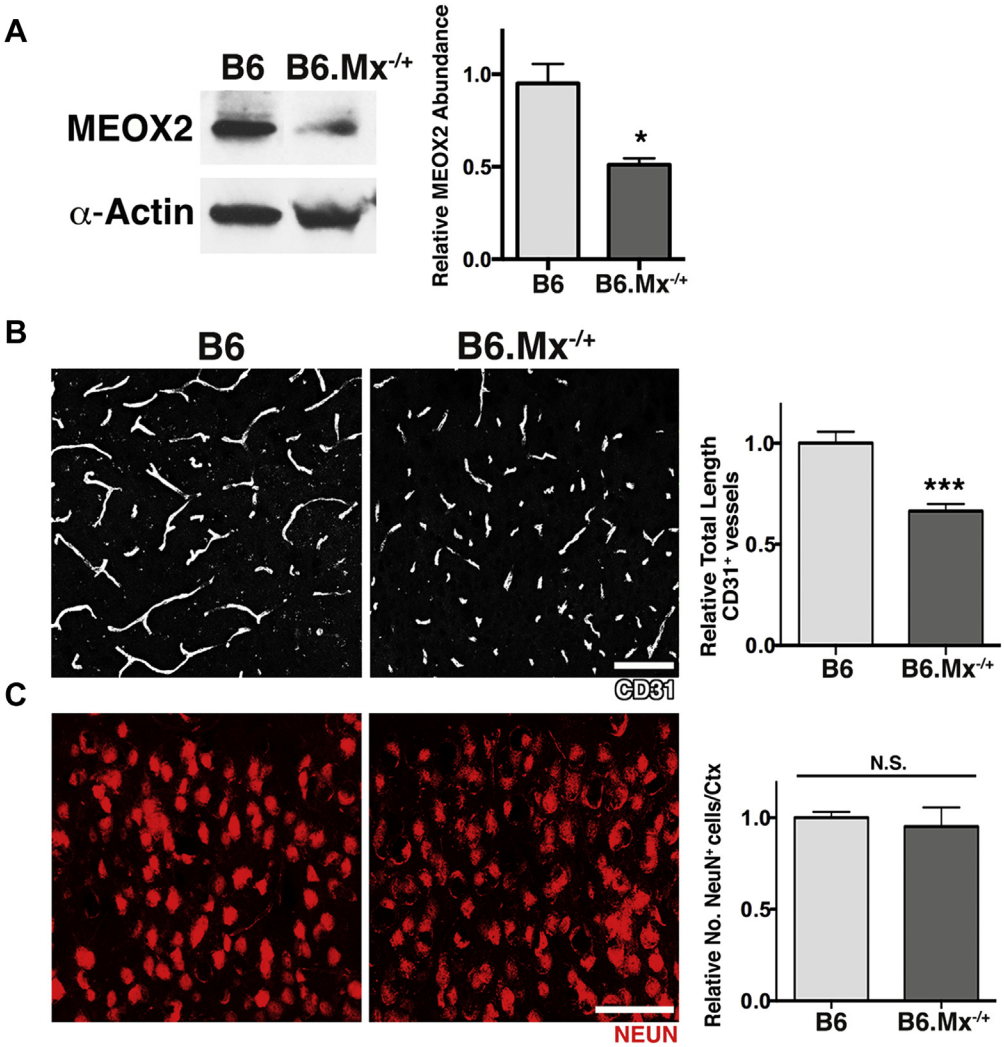

Fig. 1. Haploinsufficiency of *Meox2* expression causes reduction in microvascular density. (A) Western blot analysis showing a significant reduction (48%) of MEOX2 protein in B6.*Mx*$^{-/+}$ mice. (B) Representative images and quantitative analysis of CD31 immunostaining in the cortex of B6 and B6.*Mx*$^{-/+}$mice at 4 months of age, demonstrating a significant reduction in microvascular density. (C) Representative images and quantitative analysis of NEUN immunostaining in the cortex of B6 and B6.*Mx*$^{-/+}$ mice at 10 months of age. No changes in the number of neurons were found between groups. (A–C) Values are relative mean ± standard error of the mean to the B6 values, $n = 4$ mice per group, $^{*}p = 0.0406$, and $^{***}p = 0.0008$ by unpaired t test. Scale bars: 50 μm.

Neuron (NEUN+), microvessel (LAMA2), and plaque/microvessel (lectin) area were calculated separately. As the lectin area contained plaque and microvessel area, plaque area alone was calculated as lectin area − LAMA2 area. In all cases, area was calculated using specially designed algorithms that have been described and validated previously (Soto et al., 2015) and are available on request.

2.6. Western blotting

Protein levels of human APP in transgenic mice were measured using Western blotting. Protein sample concentration was determined via DC assay (Bio-Rad), and a total of 1.5 μg of the protein was used for this analysis. Samples were heated to 95 °C for 5 minutes and then loaded onto a 12% TGX stain-free gel (Bio-Rad). Gels were run at 150 V for 45 minutes and then transferred to a nitrocellulose membrane (Life Technologies) via the iBlot for 7 minutes. Blots were then incubated for 2 nights to a blocking solution (5% skim milk powder block in 0.1% PBS-Tween) with 6E10 antibody (1:2000, Covance/BioLegend) or Meox2 (1:1000) at 4 °C. Blots were then washed 3 times in 0.1% PBS-Tween and incubated in the appropriate secondary antibody (anti-mouse IgG 1:30,000; Millipore) for 2 hours at room temperature. Detection was carried

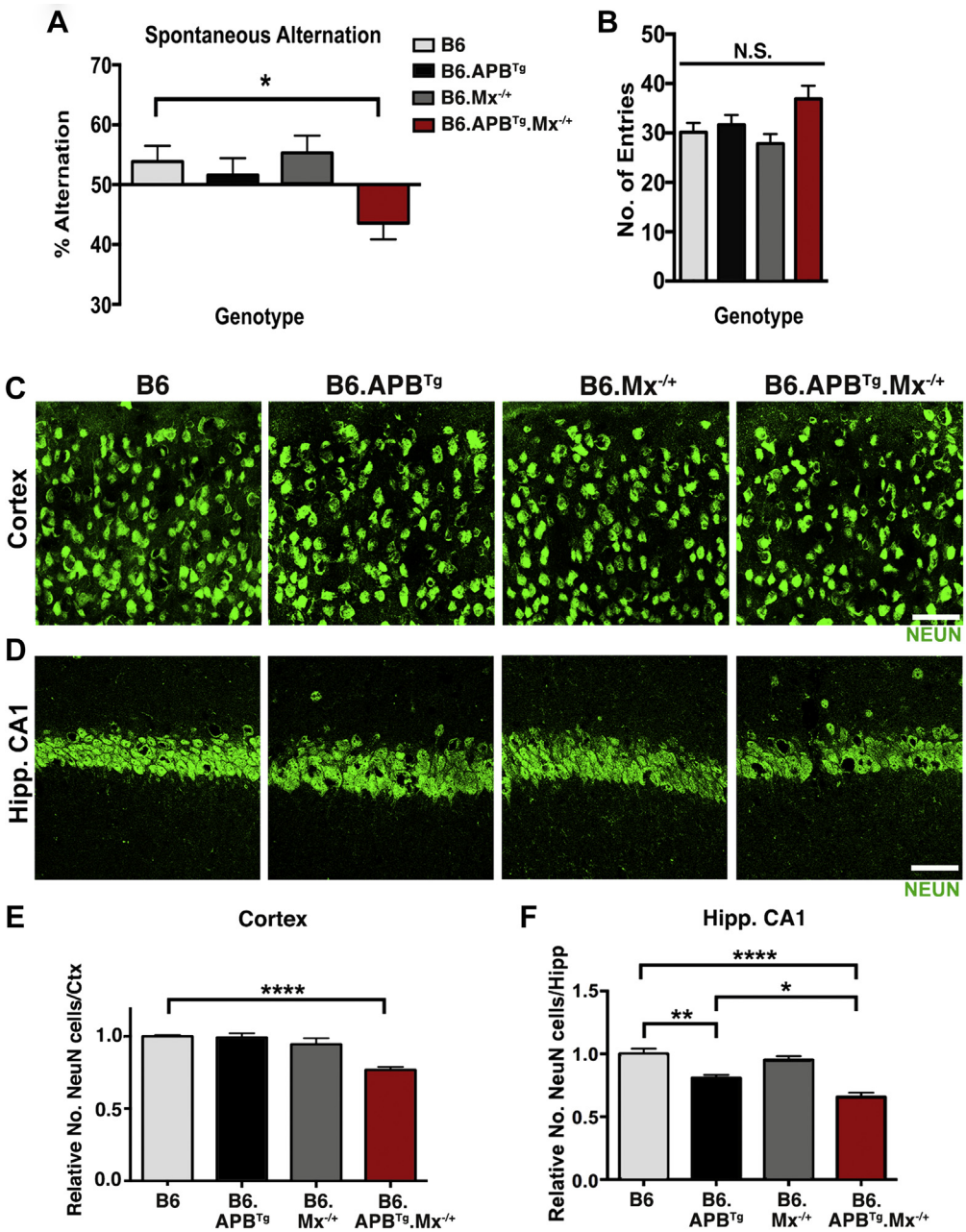

Fig. 2. Y-maze deficits and neuronal cell loss in B6.APB^{Tg}.$Mx^{-/+}$ mice. (A) Y-maze spontaneous alternation test shows significant deficits in percentage of alternation in B6.APB^{Tg}.$Mx^{-/+}$ mice compared with B6, B6.$Mx^{-/+}$, and B6.APB^{Tg} mice at 14 months of age. (B) No significant differences in the number of entries during the test were found between the groups. (C) Representative images of NEUN immunostaining in the cortex of B6, B6.APB^{Tg}, B6.$Mx^{-/+}$, and B6.APB^{Tg}.$Mx^{-/+}$ mice at 14 months of age. (D) Representative images of NEUN immunostaining in the hippocampal CA1 of B6, B6.APB^{Tg}, B6.$Mx^{-/+}$, and B6.APB^{Tg}.$Mx^{-/+}$ mice at 14 months of age. (E) Quantitative analysis of NEUN-immunostained neurons in the cortex of B6, B6.APB^{Tg}, B6.$Mx^{-/+}$, and B6.APB^{Tg}.$Mx^{-/+}$ mice at 14 months of age, showing a significant decrease of neurons in B6.APB^{Tg}.$Mx^{-/+}$ mice. (F) In the hippocampal CA1, quantitative analysis of $NEUN^{+}$ neurons shows a significant decrease in B6.APB^{Tg} and B6.APB^{Tg}.$Mx^{-/+}$ mice, compared with B6 and B6.$Mx^{-/+}$ mice. However, there is also a significant decrease in NEUN+ neurons in B6.APB^{Tg}.$Mx^{-/+}$ mice compared with B6.APB^{Tg} mice. (A and B) $n = 8$ mice per group. (E and F) $n = 4$ mice per group. (A and B) and (E and F) Values are mean ± standard error of the mean. $^{*}p < 0.05$, $^{**}p = 0.001$, and $^{****}p < 0.0001$ by 1-way analysis of variance. Scale bars: 50 μm.

out using ECL detection reagents (GE Healthcare). Blots were treated with 0.25% sodium azide, thoroughly washed, further probed with anti-beta actin (1:1000; Abcam) in 0.1% PBS-Tween overnight at 4 °C, washed 3 times, incubated with secondary antibody (anti-mouse IgG 1:30,000; Millipore) for 2 hours at room temperature, washed, and detected.

2.7. Enzyme-linked immunosorbent assay

Human $A\beta_{42}$ levels were determined using the enzyme-linked immunosorbent assay (ELISA) detection kit from Life Technologies (cat#KHB3442) following the specified instructions. Protein samples from 14–month-old mouse brains were diluted 1:50 in standard diluent buffer to ensure that urea and sodium dodecyl sulfate levels were compatible with the ELISA kit (see protein isolation details at Section 2.3). Samples were then compared with a standard curve, and Aβ42 concentrations were established against the samples' protein concentrations following manufacturer's recommendations.

2.8. Statistical analysis

Data were analyzed using GraphPad Prism software. Significance was calculated using unpaired *t* tests for comparisons between 2 groups and 1-way multifactorial analysis of variance followed by Tukey post hoc tests for multiple comparisons. *p* Values are provided as stated by GraphPad, and significance was determined with p values <0.05.

3. Results

Mice carrying only 1 copy of *Meox2* (B6.$Mx^{-/+}$ mice, see Section 2) were used to determine the contribution of *Meox2* haploinsufficiency to AD-related pathology. Western blots confirmed that MEOX2 protein levels were reduced by ~50% in the brains of 4-month-old B6.$Mx^{-/+}$ mice compared with wild-type controls (B6.$Mx^{+/+}$, Fig. 1A). A previous study reported reductions in cerebral microvessels and in cortical CBF in mice haploinsufficient for *Meox2* (Wu et al., 2005). In line with these previous findings, we also found a small but significant reduction in $CD31^+$ microvessels in our 4-month-old B6.$Mx^{-/+}$ mice compared with B6 mice (Fig. 1B). However, in contrast to previous findings, no differences in the number of cortical $NEUN^+$ neurons were found between 10-month-old-B6.$Mx^{-/+}$ and B6 mice (Fig. 1C), indicating that in the strain used here, *Meox2* haploinsufficiency alone does not affect neuronal survival. Possible explanations for these differences include choice of *Meox2* null allele and strain backgrounds.

3.1. Meox2 haploinsufficiency promotes Y-maze deficits and neuronal loss in B6.APB^{Tg} mice

Cohorts of at least 8 B6.APB^{Tg}.$Mx^{-/+}$ mice and similar numbers of littermate controls (B6, B6.$Mx^{-/+}$, and B6.APB^{Tg}) were established and aged to 14 months, and spatial working memory was examined using a Y-maze (Fig. 2A and B). At 14 months of age, a significant deficit in spontaneous alternation was seen only in B6.APB^{Tg}.$Mx^{-/+}$ mice (43.58% ± 7.75%, $p = 0.0183$) and not in the control strains (B6 = 53.85% ± 6.99%, B6.APB^{Tg} = 51.58% ± 8.03%, and B6.$Mx^{-/+}$ = 55.30% ± 6.43%). No differences in the number of entries were found between groups (Fig. 2B). Mice were harvested and neuronal cell loss assessed. NEUN-immunostained neurons were quantified in the cortex and hippocampus of B6.APB^{Tg}.$Mx^{-/+}$ mice and compared with control mice. A significant decrease in the number of $NEUN^+$ cells was found in both the cortex and hippocampus of 14-month-old B6.APB^{Tg}.$Mx^{-/+}$ mice compared with control mice (Fig. 2C–F). Interestingly, neuronal cell loss was not observed in a second cohort of 10-month-old B6.APB^{Tg}.$Mx^{-/+}$ mice (data not shown), suggesting that neuronal cell loss occurred between 10 and 14 months of age.

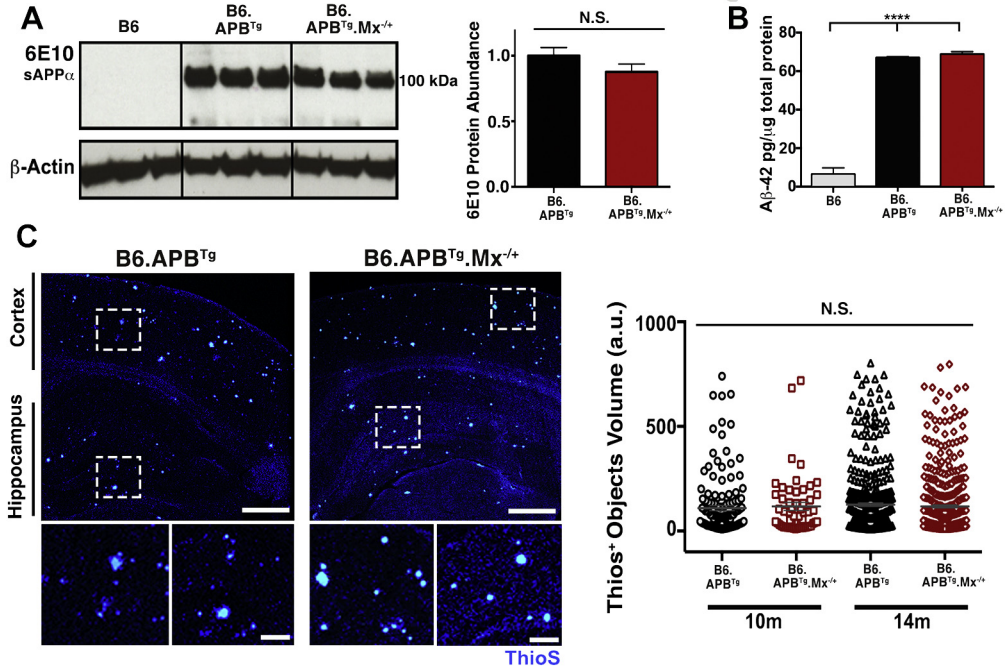

Fig. 3. *Meox2* haploinsufficiency does not alter amyloid-β (Aβ) deposition in B6.APB^{Tg}.$Mx^{-/+}$ mice. (A) Western blot analysis of soluble amyloid precursor protein (APP) using 6E10 antibody shows no significant differences between B6.APB^{Tg} and B6.APB^{Tg}.$Mx^{-/+}$ mice. (B) Quantitative analysis of $A\beta_{42}$ peptide by enzyme-linked immunosorbent assay shows no significant differences between B6.APB^{Tg} and B6.APB^{Tg}.$Mx^{-/+}$ mice. (C) Representative images and quantification of Aβ plaque deposition using ThioS staining showed no significant differences between B6.APB^{Tg} and B6.APB^{Tg}.$Mx^{-/+}$ mice. (A and B) Values are mean ± standard error of the mean, $n = 4$ mice per group, $^{****}p < 0.0001$ by 1-way analysis of variance. Scale bars: 500 μm (top panels) and 100 μm (bottom panels).

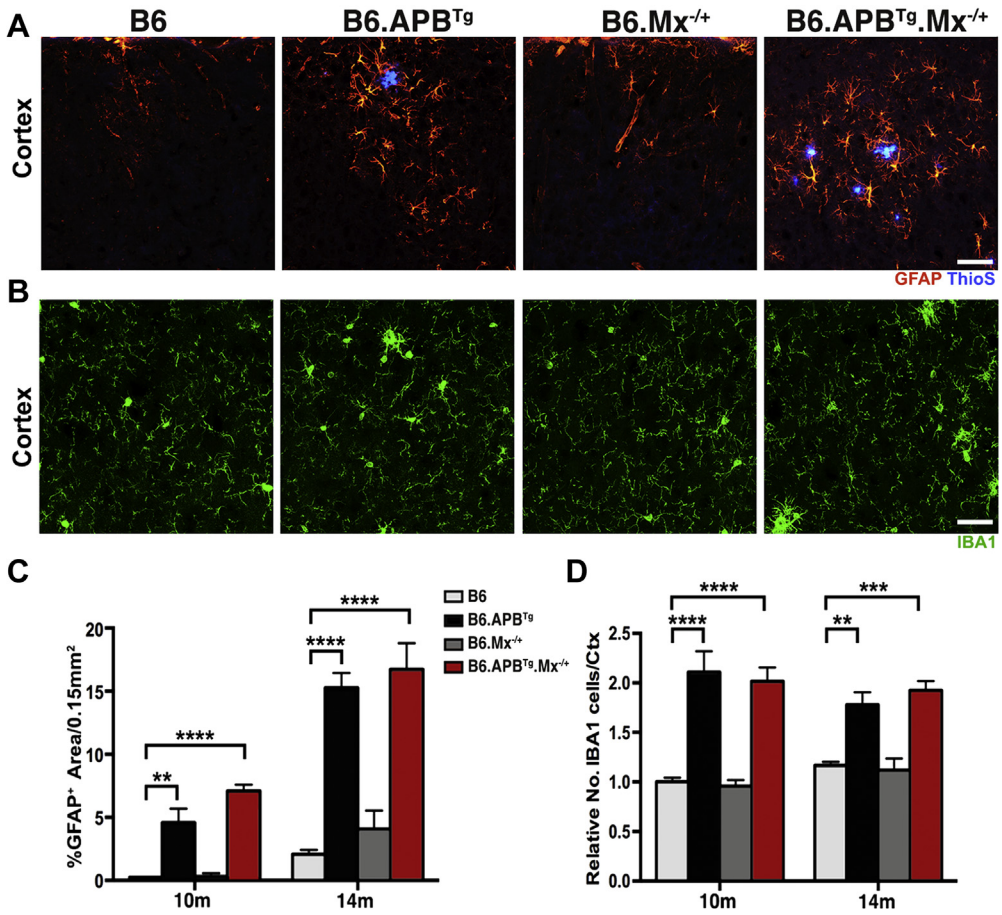

Fig. 4. *Meox2* haploinsufficiency does not alter glial activation in B6.APB^{Tg}.$Mx^{-/+}$ mice. (A) Representative images of glial fibrillary acidic protein (GFAP) immunostaining of astrocytes in the cortex of B6, B6.APB^{Tg}, B6.$Mx^{-/+}$, and B6.APB^{Tg}.$Mx^{-/+}$ mice at 14 months of age. (B) Representative images of IBA1 immunostaining of microglial cells in the cortex of B6, B6.APB^{Tg}, B6.$Mx^{-/+}$, and B6.APB^{Tg}.$Mx^{-/+}$ mice at 14 months of age. (C) Quantitative analysis of GFAP-immunolabeled area in the cortex of B6, B6.APB^{Tg}, B6.$Mx^{-/+}$, and B6.APB^{Tg}.$Mx^{-/+}$ mice at 10 and 14 months of age. Significant increases in GFAP levels were observed B6.APB^{Tg} and B6.APB^{Tg}.$Mx^{-/+}$ mice compared with B6 or B6.$Mx^{-/+}$ mice. No significant differences were observed between B6.APB^{Tg} and B6.APB^{Tg}.$Mx^{-/+}$ mice. (D) Quantitative analysis of IBA1^{+} microglial cells in the cortex of B6, B6.APB^{Tg}, B6.$Mx^{-/+}$, and B6.APB^{Tg}.$Mx^{-/+}$ mice at 10 and 14 months of age. Significant increases in IBA1+ cells were observed B6.APB^{Tg} and B6.APB^{Tg}.$Mx^{-/+}$ mice compared with B6 or B6.$Mx^{-/+}$ mice. No significant differences were observed between B6.APB^{Tg} and B6.APB^{Tg}.$Mx^{-/+}$ mice. (C and D) Values are mean ± standard error of the mean, $n = 4$ mice per group, $^{**}p < 0.01$, $^{***}p < 0.001$, and $^{****}p < 0.0001$ by 1-way analysis of variance. Scale bars: 50 μm.

3.2. *Meox2* haploinsufficiency does not alter Aβ production, plaque deposition, or glia activation in B6.APB^{Tg} mice

To begin to determine the mechanism(s) through which *Meox2* haploinsufficiency causes neuronal cell loss in B6.APB^{Tg} mice, plaque load was assessed in B6.APB^{Tg}.$Mx^{-/+}$ and B6.APB^{Tg} mice at both 10 and 14 months of age. Immunoblotting using 6E10, an antibody that binds human APP protein and its fragments, showed no significant differences in human soluble APP levels between B6.APB^{Tg}.$Mx^{-/+}$ and B6.APB^{Tg} mice (Fig. 3A). Similarly, no differences were found in human $A\beta_{42}$ levels (by ELISA, Fig. 3B) or Aβ plaque load (by Thioflavin S [ThioS] staining, Fig. 3C) between brains of B6.APB^{Tg}.$Mx^{-/+}$ and B6.APB^{Tg} mice, indicating that *Meox2* haploinsufficiency did not dramatically alter APP production or amyloid deposition. Next, astrocyte reactivity and microglial activation were assessed. Astrocyte reactivity, assessed by GFAP immunostaining, was significantly increased in the cortex of B6.APB^{Tg} and B6.APB^{Tg}.$Mx^{-/+}$ mice at both 10 and 14 months compared with B6 or B6.$Mx^{-/+}$ mice (Fig. 4A and C). However, no differences in GFAP immunostaining were found between B6.APB^{Tg} and B6.APB^{Tg}.$Mx^{-/+}$ mice at both 10 and 14 months of age. Microglial activation was assessed using IBA1, TREM2, and CD68 and was also not significantly different between B6.APB^{Tg} and B6.APB^{Tg}.$Mx^{-/+}$ mice (Figs. 4B and D and 5). Collectively, these data suggest that glial cell responses are not overtly different in B6.APB^{Tg}.$Mx^{-/+}$ compared with B6.APB^{Tg} mice.

3.3. Reduced microvessel coverage surrounding plaques correlated with increased neuronal cell loss in B6.APB^{Tg}.Mx$^{-/+}$ mice

Because *Meox2* haploinsufficiency causes reductions in microvessels from a young age (Fig. 1), we analyzed the area of microvessels (using CD31, a marker of endothelial cells, see Section 2) in the cortex and hippocampus (CA1 region) of B6.APB^{Tg}.$Mx^{-/+}$ and control mice at 10 and 14 months of age (Fig. 6A). As expected, the area of cortical and CA1 microvessels immunolabeled with CD31 was significantly reduced in both B6.APB^{Tg}.$Mx^{-/+}$ and B6.$Mx^{-/+}$ mice compared with B6 and B6.APB^{Tg} mice (Fig. 6B and C). However, compared with B6.$Mx^{-/+}$ mice, B6.APB^{Tg}.$Mx^{-/+}$ showed a further and significant reduction in CD31^{+} microvessel area in the cortex (but not in the CA1 region) (Fig. 6B and C) at 14 months of age. This suggests additional loss of cortical microvessels in B6.APB^{Tg}.$Mx^{-/+}$ mice compared with B6.$Mx^{-/+}$ mice.

Previous studies have shown that plaque deposition disrupts microvessels (Brown and Thore, 2011; Grammas et al., 2011; Kelleher and Soiza, 2013; Zlokovic, 2011). Therefore, we

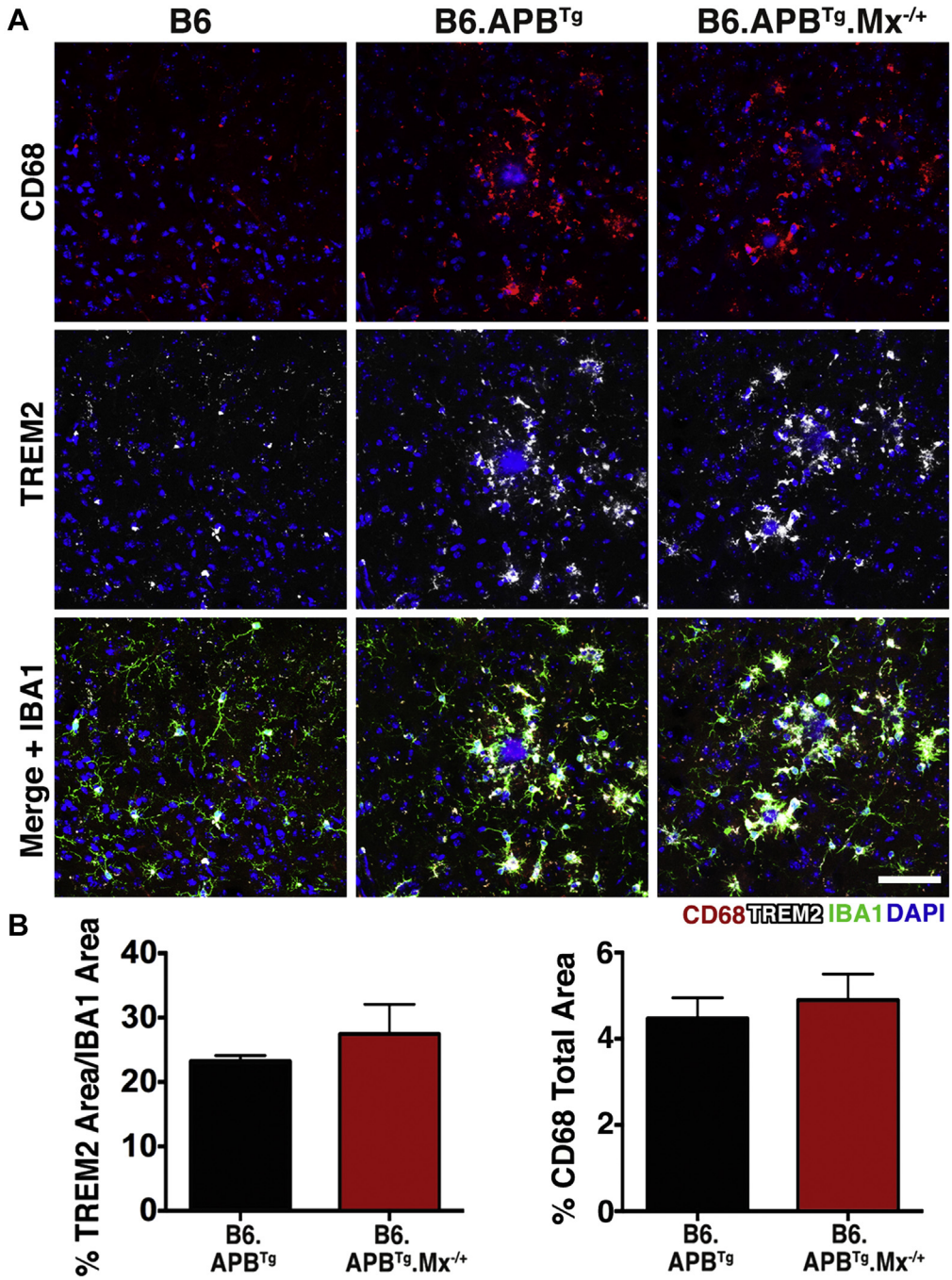

Fig. 5. Microglia are not overtly affected by *Meox2* haploinsufficiency. (A) Representative images of colocalization of CD68 and TREM2 with allograft inflammatory factor 1^+ microglial cells in B6.APB^{Tg} and B6.$APB^{Tg}.Mx^{-/+}$ mice. (B) Quantitative analyses of TREM2 and CD68 immunostained area in B6.APB^{Tg} and B6.$APB^{Tg}.Mx^{-/+}$ mice at 14 months of age. No significant differences were found between groups. (B) Values are mean ± standard error of the mean, $n = 4$ mice per group. Scale bar: 50 μm.

hypothesized that microvessel loss in B6.$APB^{Tg}.Mx^{-/+}$ mice would be greatest in regions containing plaques. To test this, brain sections from B6.$APB^{Tg}.Mx^{-/+}$ and controls at 14 months of age were immunolabeled with LAMA2, a basement membrane protein that identifies microvessels, and lectin, a protein that binds to cell membranes and conveniently labels microvessels (Mazzetti et al., 2004). In addition, strong immunoreactivity of lectin was found in microglia clusters surrounding the amyloid plaques (Fig. 7A and 8A) and when combined with LAMA2 allows simultaneous assessment of microvessel and plaque area (see Section 2). There was no significant difference in the area of $LAMA2^+$ microvessels in B6.APB^{Tg} mice compared with B6 mice (Fig. 8B). However, a significant reduction in $LAMA2^+$ microvessel area surrounding plaques was found in B6.$APB^{Tg}.Mx^{-/+}$ mice compared with B6.APB^{Tg} mice (Fig. 8B). This difference was not because of changes in plaque size (Fig. 8C). We next determined whether the combination of microvessel reduction and plaque deposition in B6.$APB^{Tg}.Mx^{-/+}$ mice could be intensifying the loss of neurons in B6.$APB^{Tg}.Mx^{-/+}$ compared with control mice. $NEUN^+$ neurons were quantified specifically in regions of activated $IBA1^+$ microglia clusters surrounding plaques (Fig. 8D). There was a significant reduction in $NEUN^+$ neurons surrounding plaques in B6.$APB^{Tg}.Mx^{-/+}$ mice

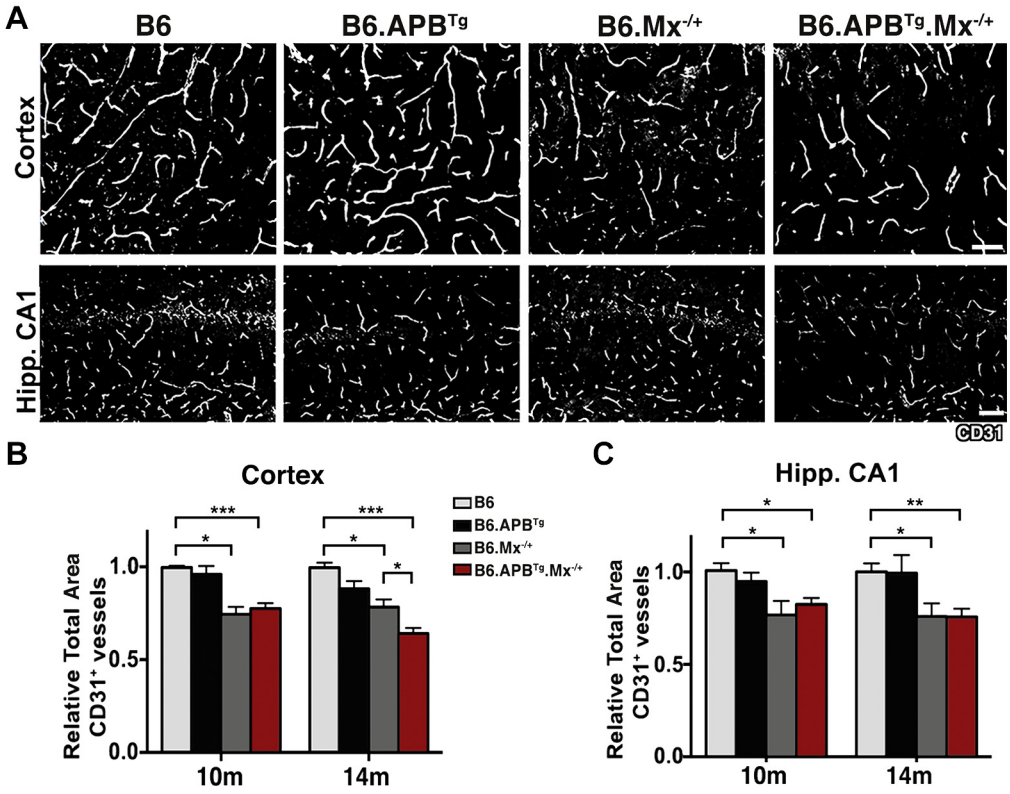

Fig. 6. *Meox2* haploinsufficiency induces endothelial cell loss in B6.APB^{Tg}.$Mx^{-/+}$ mice. (A) Representative images of CD31-immunolabeled endothelial cells in the cortex and hippocampal CA1. (B) Quantitative analysis of $CD31^{+}$ microvessel length in the cortex of B6, B6.APB^{Tg}, B6.$Mx^{-/+}$, and B6.APB^{Tg}.$Mx^{-/+}$ mice at 10 and 14 months of age. (C) Quantitative analysis of $CD31^{+}$ microvessel length in the hippocampal CA1 at 10 and 14 months of age. (B and C) Values are mean ± standard error of the mean, $n = 4$ mice per group, $^{*}p < 0.05$, $^{**}p < 0.01$, and $^{***}p < 0.001$ by 1-way analysis of variance. Scale bars: 50 μm in (A).

compared with B6.APB^{Tg} mice (Fig. 8E), which was independent of plaque area (Fig. 8F). Therefore, Meox2 haploinsufficiency and plaque deposition had a synergistic neurotoxic effect in B6.APB^{Tg}.$Mx^{-/+}$ mice.

4. Discussion

It is thought that pathologic neurovascular irregularities and vascular risk factors are important contributors to the onset and progression of AD. Several reports have shown severe pathologic changes in the cerebral vasculature (Buee et al., 1994; Farkas and Luiten, 2001; Grammas, 2011; Halliday et al., 2015; Sagare et al., 2012; Zlokovic, 2005) and associated vascular-related genetic risk factors (Bell, 2012; Winkler et al., 2015; Zhao et al., 2015; Zlokovic, 2010) with AD development and progression. Vascular-related genes have been found to be both affected by AD (e.g., *GLUT1* and *LRP*) and identified as genetic risk factors for disease development (e.g., *APOE*, *MEOX2*, *MYOCD*, and *PICALM*) (Bell, 2012; Mahley et al., 2009; Sagare et al., 2012; Zlokovic, 2010). In the case of *MEOX2*, rare copy number variants for this gene are associated with a severe form of AD in humans (Rovelet-Lecrux et al., 2012). Furthermore, MEOX2 expression is downregulated in endothelial cells from brains

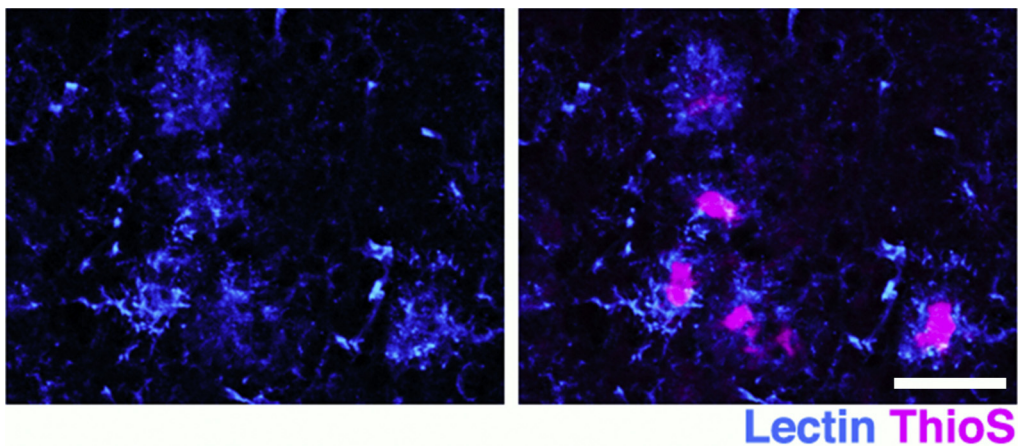

Fig. 7. ThioS+ plaques are also identified by lectin that marks microglial clusters. $ThioS^{+}$ plaque (magenta) is immunostained by lectin (blue). Scale bar: 50 μm.

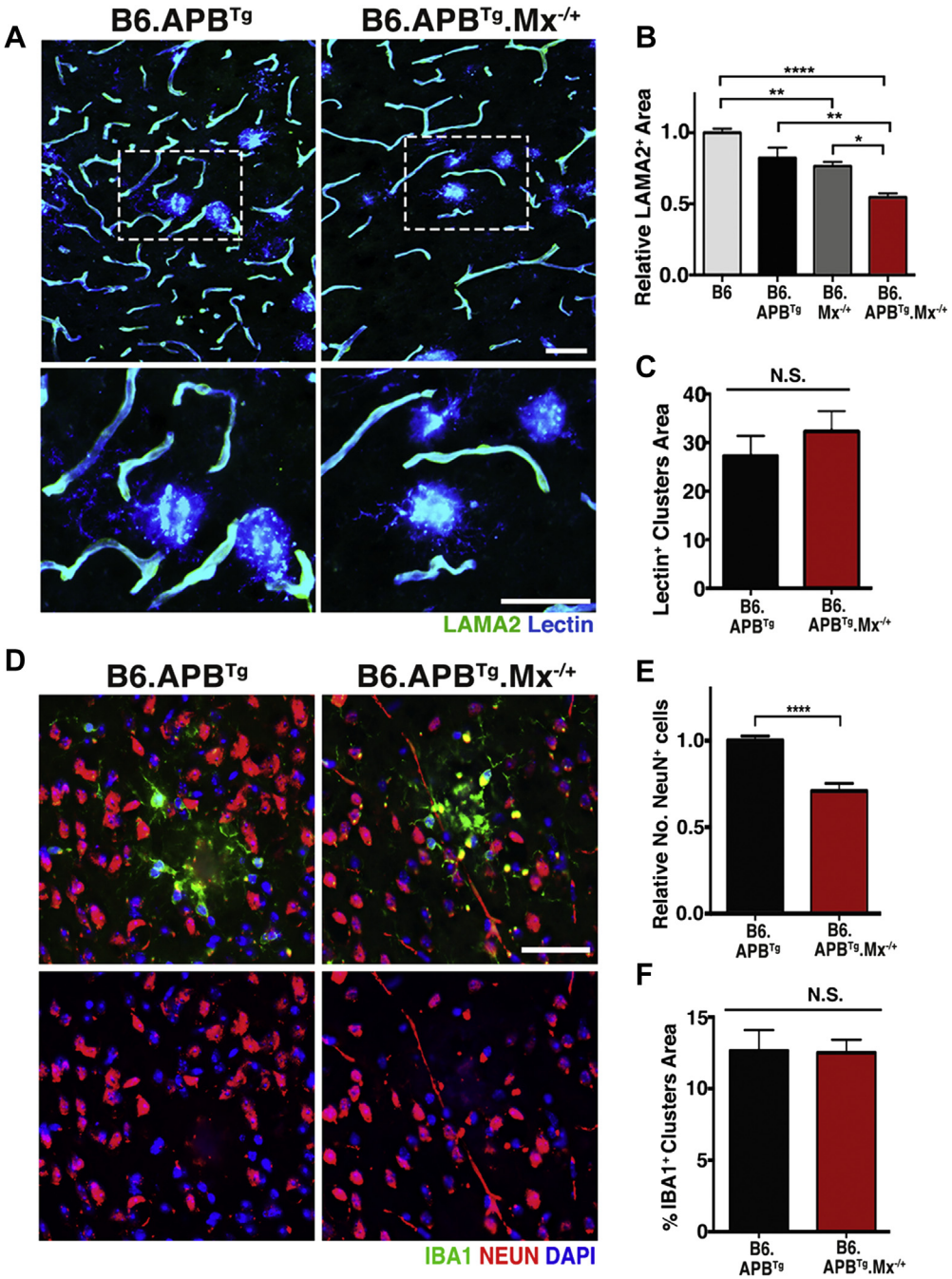

Fig. 8. Loss of microvessels in B6.APB^{Tg}.$Mx^{-/+}$ mice is more severe in plaque regions. (A) Representative images of dual immunolabeling of microvessels with laminin A2 (LAMA2) (green) and lectin (blue) in B6.APB^{Tg} and B6.APB^{Tg}.$Mx^{-/+}$ mice. Lectin is also labeling plaque clusters (see also Fig. 7). (B) Quantitative analysis of LAMA2-immunolabeled area showing a significant reduction of microvessels in regions containing plaques in B6.APB^{Tg}.$Mx^{-/+}$ mice compared with B6.APB^{Tg} mice at 14 months of age. (C) Quantitative analysis of lectin^{+} area in B6.APB^{Tg} and B6.APB^{Tg}.$Mx^{-/+}$ mice at 14 months of age. (D) Representative images of dual immunolabeling of neurons with NEUN (red) and plaque-associated microglia (green) with IBA1 in B6.APB^{Tg} and B6.APB^{Tg}.$Mx^{-/+}$ mice. (E) Quantitative analysis of NEUN-immunolabeled neurons showing a significant reduction of these cells in B6.APB^{Tg}.$Mx^{-/+}$ mice at 14 months of age. (F) Quantitative analysis of IBA1^{+} plaque cluster area in B6.APB^{Tg} and B6.APB^{Tg}.$Mx^{-/+}$ mice at 14 months of age. (B, C, E, and F) Values are mean ± standard error of the mean, $n = 4$ mice per group, $^{*}p < 0.05$, $^{**}p < 0.01$, and $^{****}p < 0.0001$ by 1-way analysis of variance. (F) $^{****}p < 0.0001$ by unpaired t test. Scale bars: 50 μm.

of AD patient, and these cells were found to be dysfunctional and pro-apoptotic in in vitro assays of vascular tube formation (Wu et al., 2005). In addition, previous studies (Wu et al., 2005), confirmed in our study here (Fig. 1), showed that haploinsufficiency of MEOX2 in mice led to microvascular reductions in the brain. Given the association of copy number variations of *MEOX2* with severe forms of AD (Rovelet-Lecrux et al., 2012), this suggests MEOX2-mediated vascular dysfunction may be a contributing factor in AD. In support of this, here we show that haploinsufficiency of *Meox2* in mice reduces cerebral vascular density and leads to neuronal loss and cognitive deficits in B6.APB^{Tg} mice.

Interestingly, no changes in plaque load or deposition were found between B6.APB^{Tg}.$Mx^{-/+}$ and B6.APB^{Tg} mice, indicating that *Meox2* haploinsufficiency in combination with plaque load caused an age-dependent degeneration of neurons in B6.APB^{Tg}.$Mx^{-/+}$ mice. Several mouse models of AD have successfully shown extensive

amyloid plaque deposition and neuroinflammation, but, in the absence of additional genetic manipulations, not many show significant neuronal loss and associated cognitive decline (Onos et al., 2015; Webster et al., 2014; Wirths and Bayer, 2010). The lack of substantial neuronal cell loss significantly limits the identification and testing of therapeutic targets for AD (Onos et al., 2015). However, recent studies have shown that combinatorial approaches that disrupt neurovascular function in addition to promoting Aβ plaque deposition can induce neuronal cell loss and some cognitive impairment (Sagare et al., 2013; Winkler et al., 2015; Zhao et al., 2015). In our study, *Meox2* haploinsufficiency caused early reductions in microvessel density that did not promote neuronal loss (Fig. 1). However, when combined with mutant APP and PSEN1 proteins, Meox2 haploinsufficiency caused significant neuronal loss (Fig. 2), particularly around plaques (Fig. 8). Interestingly, microvessel reduction and plaque deposition occurred before neuronal cell loss in B6.APB^{Tg}.$Mx^{-/+}$ mice suggesting microvessel deficiencies and amyloid deposition combine to cause neuronal cell loss in this model.

It is not clear why *Meox2* haploinsufficiency causes increased neuronal cell loss in B6.APB^{Tg}.$Mx^{-/+}$ mice compared with B6.APB^{Tg} mice. One explanation may lie in the fact that *Meox2* haploinsufficiency causes significant reductions in CBF causing hypoperfusion (Wu et al., 2005). It is possible that hypoperfusion in B6.APB^{Tg}.$Mx^{-/+}$ compared with B6.APB^{Tg} mice sensitizes neurons to Aβ toxicity, as a mild reduction in CBF can disrupt important neuronal functions, such as protein synthesis (Iadecola, 2004; Zlokovic, 2011). Furthermore, it is possible that CBF could be even more compromised in B6.APB^{Tg}.$Mx^{-/+}$ mice because of the deposition of Aβ, leading to an additional loss of microvessels and increased neuronal toxicity. An alternative explanation is that decreased levels of *Meox2* in endothelial cells may disrupt Aβ clearance. Aβ is cleared by the vascular system through the low-density lipoprotein 1 (LRP1) receptor. Reduced levels of LRP1 receptor as a result of microvessel loss would result in potential accumulation of Aβ on blood vessels (Wu et al., 2005; Zlokovic, 2010; Zlokovic et al., 2010). Although in our study, we saw no significant differences in overall plaque load between B6.APB^{Tg}.$Mx^{-/+}$ and B6.APB^{Tg} mice; therefore, this explanation seems unlikely. However, given that neurons are the main producers of mutant human APP in the mouse model used here (Borchelt et al., 1997), it is possible that B6.APB^{Tg}.$Mx^{-/+}$ has an increased ratio of APP production per neuron as we did not observe a decrease in APP levels (Fig. 3A) despite observing neuronal cell loss (Fig. 2). Interestingly, by considering the ratio of plaque load to APP-producing neuronal cell number between B6.APB^{Tg} and B6.APB^{Tg}.$Mx^{-/+}$ mice, we can propose that B6.APB^{Tg}.$Mx^{-/+}$ mice had increased plaque load compared with B6.APB^{Tg} mice. Although further investigation is required, this suggests that clearance of Aβ may be affected by *Meox2* haploinsufficiency. Irrespective of the mechanism by which *Meox2* haploinsufficiency causes neuronal cell loss, we propose it creates a more human-relevant environment. *MEOX2* expression is downregulated in endothelial cells in human AD brains (Wu et al., 2005), whereas *Meox2* is not downregulated in endothelial cells during disease progression in mouse models of AD where neuronal cell loss is not normally observed. This lack of a reduction in MEOX2 protein in mouse models of AD may cause a robustness of mouse cerebral endothelial cells in response to plaque load and override the neurotoxic effects of Aβ plaque deposition observed in humans (Deshpande et al., 2006; Donev et al., 2009; Urbanc et al., 2002; Yankner et al., 1989). This robustness could be lessened by *Meox2* haploinsufficiency, causing further loss of vascular endothelial cells and neurons in these plaque regions. This mechanism could also account for the association between copy number variations involving *MEOX2* with severe phenotypes in human AD (Rovelet-Lecrux et al., 2012).

The reduction in vascular density in the brain caused by a combination of *Meox2* haploinsufficiency and Aβ deposition could be an important contributor to cerebral hypoperfusion in AD (Brown and Thore, 2011; Farkas and Luiten, 2001; Grammas, 2011; Zlokovic, 2005). Cerebral hypoperfusion has been considered a major contributor to cognitive impairment and AD development and pathology. CBF has been seen to be reduced in the initial stages of AD when early cognitive impairment is detected, which suggests that vascular dysfunction precedes neuronal degeneration and brain atrophy (Hirao et al., 2005; Johnson et al., 2005; Pakrasi and O'Brien, 2005). One possible mechanism is that decreased CBF and altered uptake and utilization of glucose and oxygen (Brown and Thore, 2011; Farkas and Luiten, 2001; Grammas, 2011; Zlokovic, 2005) can lead to impairments in neuronal metabolism and function (Farkas and Luiten, 2001; Hermann et al., 2001; Zlokovic, 2011) causing cognitive decline and neurodegeneration.

In conclusion, our study shows that *Meox2* haploinsufficiency mediates amyloid dependent neuronal cell loss and Y-maze deficits, possibly by effecting microvessels surrounding plaques. Hence, therapies that include preservation of microvessels should be considered for human AD.

Disclosure statement

The authors have no conflicts of interest to disclose.

Acknowledgements

The authors would like to thank Kelly Keezer and Keating Pepper for help with mouse breeding and maintenance and Stacey Rizzo and members of the Mouse Neurobehavioral Phenotyping Facility at The Jackson Laboratory. This work was funded in part by The Jackson Laboratory Nathan Shock Center for Excellence in the Basic Biology of Aging, the Fraternal Order of the Eagle, the Jane B. Cook Foundation, and National Institutes of Health (NIH) R01 EY021525 (G.R.H.). W.A.G. was supported by an Institutional Development Award (IDeA) from the National Institute of General Medical Sciences of the NIH under grant number P20GM103423. The authors declare no competing financial interests.

References

Bell, R.D., 2012. The imbalance of vascular molecules in Alzheimer's disease. J. Alzheimers Dis. 32, 699–709.
Bertholet, J.Y., Crusio, W.E., 1991. Spatial and non-spatial spontaneous alternation and hippocampal mossy fibre distribution in nine inbred mouse strains. Behav. Brain Res. 43, 197–202.
Borchelt, D.R., Ratovitski, T., van Lare, J., Lee, M.K., Gonzales, V., Jenkins, N.A., Copeland, N.G., Price, D.L., Sisodia, S.S., 1997. Accelerated amyloid deposition in the brains of transgenic mice coexpressing mutant presenilin 1 and amyloid precursor proteins. Neuron 19, 939–945.
Brown, W.R., Thore, C.R., 2011. Review: cerebral microvascular pathology in ageing and neurodegeneration. Neuropathol. Appl. Neurobiol. 37, 56–74.
Buee, L., Hof, P.R., Bouras, C., Delacourte, A., Perl, D.P., Morrison, J.H., Fillit, H.M., 1994. Pathological alterations of the cerebral microvasculature in Alzheimer's disease and related dementing disorders. Acta Neuropathol. 87, 469–480.
Deshpande, A., Mina, E., Glabe, C., Busciglio, J., 2006. Different conformations of amyloid beta induce neurotoxicity by distinct mechanisms in human cortical neurons. J. Neurosci. 26, 6011–6018.
Dewey, M.E., Saz, P., 2001. Dementia, cognitive impairment and mortality in persons aged 65 and over living in the community: a systematic review of the literature. Int. J. Geriatr. Psychiatry 16, 751–761.
Donev, R., Kolev, M., Millet, B., Thome, J., 2009. Neuronal death in Alzheimer's disease and therapeutic opportunities. J. Cell Mol. Med. 13, 4329–4348.
Drew, W.G., Miller, L.L., Baugh, E.L., 1973. Effects of delta9-THC, LSD-25 and scopolamine on continuous, spontaneous alternation in the Y-maze. Psychopharmacologia 32, 171–182.
Farkas, E., Luiten, P.G., 2001. Cerebral microvascular pathology in aging and Alzheimer's disease. Prog. Neurobiol. 64, 575–611.
Gorski, D.H., Walsh, K., 2003. Control of vascular cell differentiation by homeobox transcription factors. Trends Cardiovasc. Med. 13, 213–220.

Grammas, P., 2011. Neurovascular dysfunction, inflammation and endothelial activation: implications for the pathogenesis of Alzheimer's disease. J. Neuroinflammation 8, 26.
Grammas, P., Tripathy, D., Sanchez, A., Yin, X., Luo, J., 2011. Brain microvasculature and hypoxia-related proteins in Alzheimer's disease. Int. J. Clin. Exp. Pathol. 4, 616–627.
Halliday, M.R., Rege, S.V., Ma, Q., Zhao, Z., Miller, C.A., Winkler, E.A., Zlokovic, B.V., 2015. Accelerated pericyte degeneration and blood-brain barrier breakdown in apolipoprotein E4 carriers with Alzheimer's disease. J. Cereb. Blood Flow Metab. 36, 216–227.
Hermann, D.M., Kilic, E., Hata, R., Hossmann, K.A., Mies, G., 2001. Relationship between metabolic dysfunctions, gene responses and delayed cell death after mild focal cerebral ischemia in mice. Neuroscience 104, 947–955.
Hirao, K., Ohnishi, T., Hirata, Y., Yamashita, F., Mori, T., Moriguchi, Y., Matsuda, H., Nemoto, K., Imabayashi, E., Yamada, M., Iwamoto, T., Arima, K., Asada, T., 2005. The prediction of rapid conversion to Alzheimer's disease in mild cognitive impairment using regional cerebral blood flow SPECT. Neuroimage 28, 1014–1021.
Hooper, N., Fraser, C., Stone, T.W., 1996. Effects of purine analogues on spontaneous alternation in mice. Psychopharmacology (Berl) 123, 250–257.
Hughes, R.N., 2004. The value of spontaneous alternation behavior (SAB) as a test of retention in pharmacological investigations of memory. Neurosci. Biobehav. Rev. 28, 497–505.
Iadecola, C., 2004. Neurovascular regulation in the normal brain and in Alzheimer's disease. Nat. Rev. Neurosci. 5, 347–360.
Jacquelin, C., Strazielle, C., Lalonde, R., 2012. Spontaneous alternation and spatial learning in Dab1scm (scrambler) mutant mice. Brain Res. Bull. 87, 383–386.
Jankowsky, J.L., Fadale, D.J., Anderson, J., Xu, G.M., Gonzales, V., Jenkins, N.A., Copeland, N.G., Lee, M.K., Younkin, L.H., Wagner, S.L., Younkin, S.G., Borchelt, D.R., 2004. Mutant presenilins specifically elevate the levels of the 42 residue beta-amyloid peptide in vivo: evidence for augmentation of a 42-specific gamma secretase. Hum. Mol. Genet. 13, 159–170.
Johnson, N.A., Jahng, G.H., Weiner, M.W., Miller, B.L., Chui, H.C., Jagust, W.J., Gorno-Tempini, M.L., Schuff, N., 2005. Pattern of cerebral hypoperfusion in Alzheimer disease and mild cognitive impairment measured with arterial spin-labeling MR imaging: initial experience. Radiology 234, 851–859.
Kelleher, R.J., Soiza, R.L., 2013. Evidence of endothelial dysfunction in the development of Alzheimer's disease: is Alzheimer's a vascular disorder? Am. J. Cardiovasc. Dis. 3, 197–226.
Knopman, D.S., Roberts, R., 2010. Vascular risk factors: imaging and neuropathologic correlates. J. Alzheimers Dis. 20, 699–709.
Mahley, R.W., Weisgraber, K.H., Huang, Y., 2009. Apolipoprotein E: structure determines function, from atherosclerosis to Alzheimer's disease to AIDS. J. Lipid Res. 50 (Suppl), S183–S188.
Mazzetti, S., Frigerio, S., Gelati, M., Salmaggi, A., Vitellaro-Zuccarello, L., 2004. Lycopersicon esculentum lectin: an effective and versatile endothelial marker of normal and tumoral blood vessels in the central nervous system. Eur. J. Histochem. 48, 423–428.
Norton, S., Matthews, F.E., Barnes, D.E., Yaffe, K., Brayne, C., 2014. Potential for primary prevention of Alzheimer's disease: an analysis of population-based data. Lancet Neurol. 13, 788–794.
Onos, K.D., Sukoff Rizzo, S.J., Howell, G.R., Sasner, M., 2015. Toward more predictive genetic mouse models of Alzheimer's disease. Brain Res. Bull. 122, 1–11.
Pakrasi, S., O'Brien, J.T., 2005. Emission tomography in dementia. Nucl. Med. Commun. 26, 189–196.
Rovelet-Lecrux, A., Legallic, S., Wallon, D., Flaman, J.M., Martinaud, O., Bombois, S., Rollin-Sillaire, A., Michon, A., Le Ber, I., Pariente, J., Puel, M., Paquet, C., Croisile, B., Thomas-Anterion, C., Vercelletto, M., Levy, R., Frebourg, T., Hannequin, D., Campion, D.Investigators of the GMAJ Project, 2012. A genome-wide study reveals rare CNVs exclusive to extreme phenotypes of Alzheimer disease. Eur. J. Hum. Genet. 20, 613–617.
Sagare, A.P., Bell, R.D., Zhao, Z., Ma, Q., Winkler, E.A., Ramanathan, A., Zlokovic, B.V., 2013. Pericyte loss influences Alzheimer-like neurodegeneration in mice. Nat. Commun. 4, 2932.
Sagare, A.P., Bell, R.D., Zlokovic, B.V., 2012. Neurovascular dysfunction and faulty amyloid beta-peptide clearance in Alzheimer disease. Cold Spring Harb. Perspect. Med. 2, a011452.
Sengillo, J.D., Winkler, E.A., Walker, C.T., Sullivan, J.S., Johnson, M., Zlokovic, B.V., 2013. Deficiency in mural vascular cells coincides with blood-brain barrier disruption in Alzheimer's disease. Brain Pathol. 23, 303–310.
Soto, I., Graham, L.C., Richter, H.J., Simeone, S.N., Radell, J.E., Grabowska, W., Funkhouser, W.K., Howell, M.C., Howell, G.R., 2015. Apoe stabilization by exercise prevents aging neurovascular dysfunction and complement induction. PLoS Biol. 13, e1002279.
Urbanc, B., Cruz, L., Le, R., Sanders, J., Ashe, K.H., Duff, K., Stanley, H.E., Irizarry, M.C., Hyman, B.T., 2002. Neurotoxic effects of thioflavin S-positive amyloid deposits in transgenic mice and Alzheimer's disease. Proc. Natl. Acad. Sci. U. S. A. 99, 13990–13995.
Webster, S.J., Bachstetter, A.D., Nelson, P.T., Schmitt, F.A., Van Eldik, L.J., 2014. Using mice to model Alzheimer's dementia: an overview of the clinical disease and the preclinical behavioral changes in 10 mouse models. Front Genet. 5, 88.
Winkler, E.A., Nishida, Y., Sagare, A.P., Rege, S.V., Bell, R.D., Perlmutter, D., Sengillo, J.D., Hillman, S., Kong, P., Nelson, A.R., Sullivan, J.S., Zhao, Z., Meiselman, H.J., Wenby, R.B., Soto, J., Abel, E.D., Makshanoff, J., Zuniga, E., De Vivo, D.C., Zlokovic, B.V., 2015. GLUT1 reductions exacerbate Alzheimer's disease vasculo-neuronal dysfunction and degeneration. Nat. Neurosci. 18, 521–530.
Wirths, O., Bayer, T.A., 2010. Neuron loss in transgenic mouse models of Alzheimer's disease. Int. J. Alzheimers Dis. http://dx.doi.org/10.4061/2010/723782.
Wu, Z., Guo, H., Chow, N., Sallstrom, J., Bell, R.D., Deane, R., Brooks, A.I., Kanagala, S., Rubio, A., Sagare, A., Liu, D., Li, F., Armstrong, D., Gasiewicz, T., Zidovetzki, R., Song, X., Hofman, F., Zlokovic, B.V., 2005. Role of the MEOX2 homeobox gene in neurovascular dysfunction in Alzheimer disease. Nat. Med. 11, 959–965.
Yankner, B.A., Dawes, L.R., Fisher, S., Villa-Komaroff, L., Oster-Granite, M.L., Neve, R.L., 1989. Neurotoxicity of a fragment of the amyloid precursor associated with Alzheimer's disease. Science 245, 417–420.
Zhao, Z., Sagare, A.P., Ma, Q., Halliday, M.R., Kong, P., Kisler, K., Winkler, E.A., Ramanathan, A., Kanekiyo, T., Bu, G., Owens, N.C., Rege, S.V., Si, G., Ahuja, A., Zhu, D., Miller, C.A., Schneider, J.A., Maeda, M., Maeda, T., Sugawara, T., Ichida, J.K., Zlokovic, B.V., 2015. Central role for PICALM in amyloid-beta blood-brain barrier transcytosis and clearance. Nat. Neurosci. 18, 978–987.
Zlokovic, B.V., 2005. Neurovascular mechanisms of Alzheimer's neurodegeneration. Trends Neurosci. 28, 202–208.
Zlokovic, B.V., 2010. Neurodegeneration and the neurovascular unit. Nat. Med. 16, 1370–1371.
Zlokovic, B.V., 2011. Neurovascular pathways to neurodegeneration in Alzheimer's disease and other disorders. Nat. Rev. Neurosci. 12, 723–738.
Zlokovic, B.V., Deane, R., Sagare, A.P., Bell, R.D., Winkler, E.A., 2010. Low-density lipoprotein receptor-related protein-1: a serial clearance homeostatic mechanism controlling Alzheimer's amyloid beta-peptide elimination from the brain. J. Neurochem. 115, 1077–1089.